Self-compression of stimulated Raman backscattering by a flying focus

Z. Wu, Y. Zuo, Z. Zhang, X. Wang, J. Mu, X. D. Wang, B. Hu, J. Su, and Z. Li
Science and Technology on Plasma Physics Laboratory, Research Center of Laser Fusion, China Academy of Engineering Physics, Mianyang, Sichuan 621900, China

X. Wei
Zhongshan Photon Science, ZhongShan, Guangdong 517465, China

X. Zeng*
Science and Technology on Plasma Physics Laboratory, Research Center of Laser Fusion, China Academy of Engineering Physics, Mianyang, Sichuan 621900, China and Zhongshan Photon Science, ZhongShan, Guangdong 517465, China

(Received 22 November 2021; revised 4 July 2022; accepted 8 September 2022; published 29 September 2022)

The regime of self-compression has been proposed for plasma-based backward Raman amplification upon a flying focus. By using a pumping focus moving with a speed equal to the group velocity of stimulated Raman backscattering (SRBS), only a short part of SRBS which always synchronizes with the flying focus can be amplified. Therefore, instead of a short pulse, plasma noise or a long pulse can seed the BRA amplifiers. Here we demonstrate the regime by 2D particle-in-cell simulations, showing that the pump pulse is compressed from 26 ps to 116 fs, with an output amplitude comparable with the case of a well-synchronized short seed. As only one laser pulse is used in the simulation, the results present a significant path to simplify the Raman amplifiers.

DOI: 10.1103/PhysRevE.106.035209

I. INTRODUCTION

Currently, the peak laser power of multiple petawatts has been reported by large laser facilities relying on chirped pulse amplification [1]. A further enhancement of the laser power is impeded by the material damage of compression gratings. The difficulty can be overcome by using plasma for the gain medium due to its robustness against strong optical field. The plasma amplifiers, based on backward Raman amplification (BRA) [2–7] or strongly coupled stimulated Brillouin scattering (scSBS) [8–11] have shown the potential of generating unfocused laser intensity over 10^{17} W/cm^2, indicating exawatt(10^{18} W) laser power can be obtained within centimeter-diameter amplifiers.

The BRA experiments have shown that the amplified seed intensity far exceeded that of the pump, however, the transfer efficiency (6.4% for double passes and 5.1% for a single pass) [7,12,13] and pump depletion (more than 70% of the pump energy remained) were still low. A significant explanation for the low efficiency is the plasma heating by the pump before the seed arrived. Plasma heating can disturb the plasma wave by accelerating the electrons close to its phase velocity (about c/20). As a consequence, BRA would be suppressed by several negative effects such as particle trapping, Landau damping, and plasma wave breaking. Moreover, as multiple pulses were used for the experiments, the transfer efficiency was limited by the experimental complexity.

Flying focus has been proposed to overcome these issues [14,15]. It is able to move with an artificial velocity by chromatically focusing a chirp laser pulse. With the focusing laser intensity just above the ionization threshold of the background gas, an ionization wave is generated with a moving velocity equal to that of the flying focus [16]. For a flying velocity around $v = -c$, the Raman amplification can always be arranged just behind the ionization wave. Therefore, a clean environment, without pump heating and precursors, is created in front of the seed. Furthermore, a seedless Raman amplifier can be formed by using a flying focus [17]. For a flying focus having a velocity $v = -c$, the plasma noise is effective to a short seed because only a short part of the noise always synchronizing with the flying focus can be amplified, as shown in Fig. 1. In this way, the experiment can be significantly simplified because only one laser pulse is applied. However, the previous studies were based on one-dimensional (1D) fluid simulation, which can neither fully describe the flying focus nor the plasma instabilities. In this paper, we show the 2D particle-in-cell (PIC) simulation of seedless BRA with flying focus.

The paper is organized as follows: First, the mathematic model for flying focus is figured out and employed into the PIC mode Opic2D [18–20]. Second, the thermal effect and numerical noise with flying focus are investigated by the PIC code. Third, the competition between major plasma instabilities is analyzed. Next, a series of numerical simulations are carried out to obtain the optimal result for the seedless BRA. Finally, several key issues in the scheme are discussed and possible solutions are given.

*zxm7311@sina.com

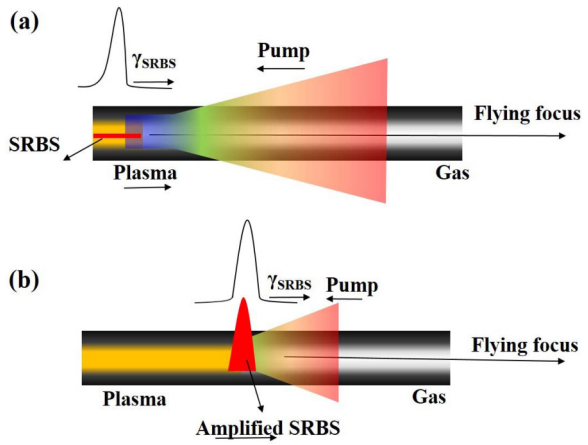

FIG. 1. Illustration of the self-compression regime due to SRBS by flying focus. The flying focus with a growth curve is set the same velocity (c) as SRBS but counter to the pump velocity ($-c$). (a) The plasma and SRBS is initially created at the entrance by flying focus. (b) The SRBS propagating with flying focus is amplified to a short pulse.

II. NUMERICAL MODEL

In general, flying focus can be described by focusing a collimated laser beam with chirp and pulse group delay (PDG). In the limit of large pulse chirp, the spatiotemporal vector potential of the flying focus can be estimated as [21,22]

$$\tilde{a}(z,t') = a(z,t)\exp[-i\phi(z,t')], \tag{1}$$

with

$$a(z,t') = \frac{a_0 W_0}{W(z,t')}\exp\left[-\frac{(t-t'/\beta)^2}{T^2} - \frac{r^2}{W(z,t')^2}\right] \tag{2}$$

and

$$\phi(z,t') = \arctan[z(t')] + \frac{Z_R k r^2}{2z(t')[1+z(t')^2/Z_R^2]} + \frac{t'^2}{2\beta}, \tag{3}$$

where $\tilde{a}(z,t')$ is the vector potential of the laser normalized by the unit of $m_e c^2/e$; m_e and e are the electron mass and charge, c is the light velocity in vacuum, $a(z,t')$ is the amplitude of $\tilde{a}(z,t')$ with the peak value of a_0, W_0 is the beam waist, $W(z,t') = W_0\sqrt{1+z(t')^2/Z_R^2}$ is beam radius at $1/e$ amplitude, T is the pulse duration at $1/e$ amplitude, $t' = t - z/c$ stands for the time in the variable moving with a velocity of c, $z(t') = Z_R t'\tau/\beta - z$, β is the pulse chirp, τ is the parameter of PGD, and z_R is the Rayleigh length. The beam waist locates at the position of $z = t'\tau z_R/\beta$ for $z(t') = 0$, indicating the focal spot is not static but variable along the propagating direction. By adjusting the pulse chirp β and τ, it can obtain subluminal to superluminal focal spots [15,21,23].

The flying focus is employed to the PIC code by setting the boundary condition of the pump as the function of time, as shown in Eqs. (1)–(3). For a moving window with velocity of v_g, t' should be changed to $t - z/c + z/v_g$ in the new variable. In the simulation, we first set a static focus in the moving window, then slightly changed the boundary condition to adjust the flying velocity.

By employing a flying focus to a 2D PIC code Opic2D, the simulations of seedless BRA were carried out in a moving window of $600\lambda \times 100\lambda$ for the z-y plane, with cells of $\Delta_z = 0.1\lambda$ and $\Delta_y = 0.2\lambda$, and 16×2 particles for each cell, where z and y are longitudinal and transverse directions, respectively, and $\lambda = 1\,\mu$m is the pump wavelength. A 4-mm-long and 50-μm-wide hydrogen is applied for the background gas. The hydrogen volume is half of the simulation window to save the computing time because less particles are calculated. Actually, the results show little difference with the hydrogen filling the simulation window. The total pump duration is about 26 ps to cover twice the 4-mm-long plasma. The initial pump focus has a waist of 5 μm, with a peak amplitude of 0.02. After it propagates through the moving window, the beam waist is magnified to about 10 μm due to the effect of ionization-induced defocusing, so the peak amplitude is reduced to 0.01, which is slightly above the ionization threshold of hydrogen, as shown in Fig. 2(a). For a clean environment in front of SRBS, the background gas at the right boundary of the moving window is kept neutral, as shown in the plasma density [Fig. 2(b)] obtained by an Ammosov-Delone-Krainov tunnel ionization model.

The thermal effect during the SRBS amplification is investigated by the PIC simulation. As the simulation starts from the background gas, the initial particle temperature is close to zero. Although the thermal effect can be mitigated by a flying focus, the plasma can still be preheated by the pump during the ionizing and propagating process before the SRBS. To illustrate this effect, the thermal effect is simulated with the flying focus shown in Fig. 2(a) at $n_{e0} = 0.02n_c$, where n_{e0} is the average plasma density, $n_c = \omega_a^2 m_e/4\pi e^2$ is the critical plasma density, ω_a is the pump frequency. The distribution of SRBS and electron energy at $t = 4000\,T$ are given in Fig. 2(c), showing a peak energy of ~1600 eV at the SRBS position. However, the electron energy cannot always represent the electron temperature because it also contains the vibration energy in the laser field. To exclude this factor, we turned off the pump at an earlier time ($t = 3900\,T$) and observed the electron energy before SRBS. The electron temperate increases from 0 to ~50 eV, a value close to the optimal one of Raman amplification [14], as shown by the brown curve in Fig. 2(d). Comparatively, the plasma temperature with static focus does not have a peak because the generated SRBS is small (cannot be accumulated as that of the flying focus), as shown by the blue curve in Fig. 2(d). However, it reaches ~200 eV due to the continuously heating, displaying a much more serious preheating effect than the case of flying focus.

As thermal noise forms the initial seed for the SRBS amplification, it has to be correctly figured out in the PIC simulation. However, it is usually covered by the inherent numerical noise of the PIC simulation. Commonly, more particles per cell (N) are used to reduce the numerical noise. As shown in Fig. 3(a), the noisy plasma wave (the longitudinal electric field E_z) without a laser decreases near three orders of magnification as N increases from 4 to 1024. Actually, the thermal noise can always be precisely approached if N is sufficiently large. However, it makes the calculation too huge to be finished. Instead, an extra interaction length can be estimated for the PIC simulation because the amplification

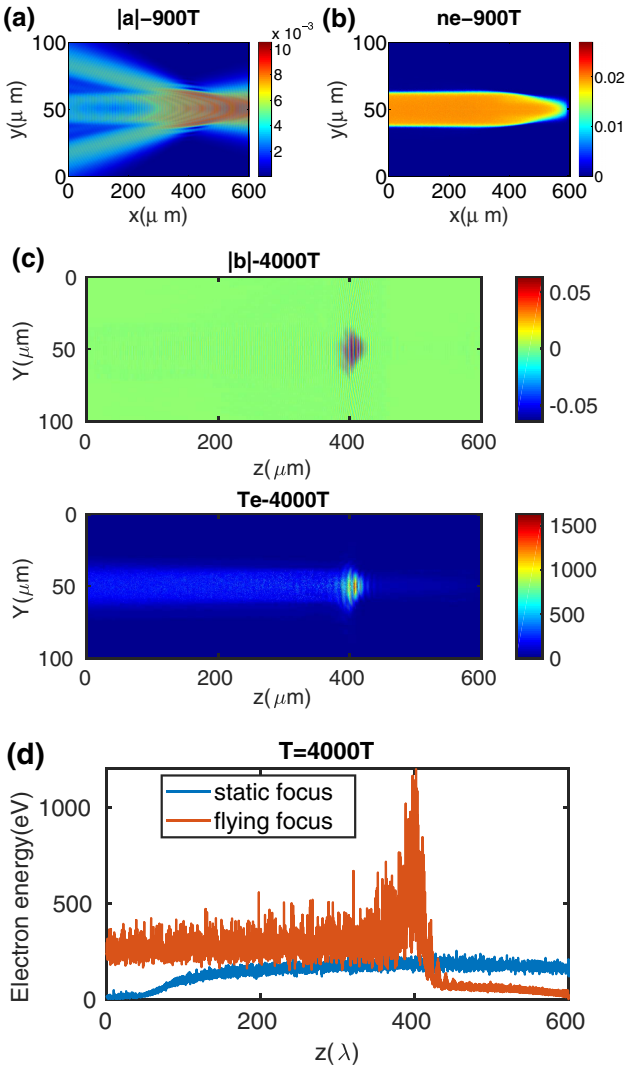

FIG. 2. (a) Distribution of flying focus at $t = 900\,T$, where $T = 3.3$ fs is the single cycle of 1 μm laser, $|a|$ is the absolute value of the pump amplitude. The velocity of flying focus and the moving window is the same (0.99c), so the focus is almost static in the simulation window. (b)Plasma density at $t = 900\,T$, the gas at right boundary of the moving window is kept neutral. (c) 2D distribution of the SRBS amplitude and electron energy obtained by flying focus at $t = 4000\,T$, where $|b|$ is the absolute value of the SRBS amplitude. (d) Comparison of the electron temperature with static and flying focus at $t = 4000\,T$

from the thermal noise to the numerical noise is very close to the ideal linear stage. For the linear SRBS amplification, it can be estimated as

$$L = \ln\left(\frac{b_n}{b_s}\right)\frac{c}{\gamma}, \tag{4}$$

where $\gamma = a\sqrt{\omega_a\omega_p}/2$ is the resonant growth rate, $\omega_p = \sqrt{4\pi n_{e0}e^2/m_e}$ is frequency of the plasma wave, b_s and b_n are the initial seed formed by thermal and numerical noise, respectively. b_n can be directly obtained from the PIC code,

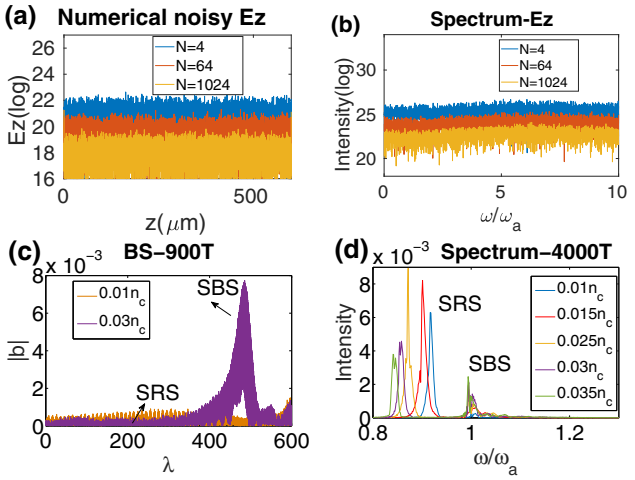

FIG. 3. (a) Numerical noise of the plasma wave (E_z) with different N at $T_e = 50$ eV, $n_{e0} = 0.02n_c$. (b) Spectra intensity of the numerical noisy E_z with different N at $T_e = 50$ eV, $n_{e0} = 0.02n_c$. (c) On-axial $|b|$ at $t = 900\,T$ for plasma density of $0.015n_c$ and $0.03n_c$. (d) Spectrum of on-axial $|b|$ developing from plasma noise at different plasma densities. In the simulation, $|b|$ is the absolute value of the SRBS amplitude, also normalized by the unit of m_ec^2/e, $a_0 = 0.01$.

and b_s is given as [24]

$$b_s \approx a\sqrt{\frac{W_{eT}}{W_{ek}}} = \frac{ae}{m_ec^2}\sqrt{\frac{T_e}{8\pi\varepsilon_0\lambda}}, \tag{5}$$

where T_e is the electron temperature, ε_0 is the permittivity of free space, $W_{eT} \sim \frac{T_e\omega_p\omega_a}{4\pi\lambda}$ and $W_{ek} \sim \frac{I_0\omega_p}{\omega_a}$ are the energy density of Langmuir wave for the equilibrium thermal noise and pump depletion, respectively, I_0 is the pump intensity. For instance, $a_0 = 0.01$, $n_{e0} = 0.02n_c$, $T_e = 50$ eV, $\lambda = 1\,\mu$m, b_s is about $b_n/4000$, according to Eq. (5). It agrees well with the result given in Ref. [26].

As the noise is used for the SRBS seed, the competition of the plasma instabilities should be taken into account. Beside RSBS, there are several typical plasma instabilities in plasma including forward Raman scattering (FRS) with a growth rate of $\gamma_{rfs} = b\omega_p^2/2\sqrt{2}\omega_a$, modulation instability (MD) with $\gamma_{\rm MD} = b^2\omega_p^2/2\omega_a$, SBS with $\gamma_{\rm SBS} = \frac{1}{2\sqrt{2}}\frac{k_a a\omega_{pi}}{\omega_a k_a c_s}$ and its strongly coupling regime with $\gamma_{\rm scSBS} = \frac{\sqrt{3}}{2}(\frac{k_a^2a^2\omega_{pi}^2}{2\omega_a})^{1/3}$, where b is the seed amplitude, k_a is the pump wave number, $\omega_{pi} = \sqrt{4\pi n_iZ^2e^2/m_i}$ is the frequency of the ion-acoustic wave, n_i and m_i are the ion density and mass, respectively, Z is the ion charge, $c_s = \sqrt{2T_e/m_i}$ is the ion-acoustic velocity [8,25]. Among these instabilities, FRS and MD mainly occur when the seeds have already grown, but have little influence on the instability competition in the initial stage. SBS and scSBC have an advantage in high density plasma as $\gamma_{\rm SBS} \propto n_{e0}^{1/2}$ and $\gamma_{\rm scSBS} \propto n_{e0}^{1/3}$ while the SRBS growth rate $\gamma \propto n_{e0}^{1/4}$. Although the numerical noise in the PIC code is much higher than the thermal noise, it does not influence the results of instability competition because all frequencies of the noisy plasma wave (E_z) are almost equally magnified(∼1000 times with N increasing from 4 to 1024), as shown in

TABLE I. Amplified peak absolute values of SRBS amplitudes ($|b|_{\max}$) at $t = 4000\,T$ with various values of plasma densities (n_{e0}), focus velocities (v_{focus}), and plasma fluctuations($\delta n_e/n_{e0}$).

$n_{e0}(n_c)$	0.01	0.015	0.02	0.025	0.03
$\|b\|_{\max}$	0.043	0.066	0.06	0.052	0.042
v_{focus}(c)	0.98	0.99	1	1.02	1.05
$\|b\|_{\max}$	0.053	0.066	0.066	0.038	0.027
$\delta n_e/n_{e0}$	0	0.05	0.1	0.2	0.3
$\|b\|_{\max}$	0.066	0.064	0.058	0.050	0.047

Fig. 3(b). Actually, the frequencies of the amplified seeds in the PIC simulation with $N = 4$ and $N = 64$ are also quite similar.

III. SIMULATION RESULTS

A series of simulations were carried out with various plasma densities, focal velocities, and plasma fluctuations as shown in Table I. First, by varying plasma densities, the maximum amplification is obtained at $n_{e0} = 0.015n_c$. For $n_{e0} \geqslant 0.03n_c c$, SRBS starts to be impacted by the SBS, as shown in Figs. 3(c) and 3(d). Second, for different flying velocities, the optimal amplification is obtained at the value of $0.99c - c$, which is close to the group velocity of SRBS at $n_{e0} = 0.015n_c$. Third, the tolerance to plasma inhomogeneity for the noisy amplification is given in Table I. In plasma with density departing from the resonant condition, the SRBS would be suppressed by the frequency detuning which makes the linear SRBS growth rate to $\gamma' = \sqrt{\gamma^2 - \delta\omega_p^2/4}$ [26], where $\delta\omega_p = \frac{1}{2}\omega_p \delta n_{e0}/n_{e0}$ is the frequency detuning. It demands $\delta\omega < 2\gamma$ for a positive SRBS growth rate, corresponding to $\delta n_{e0}/n_{e0} < 4a_0 n_{e0}/n_c \approx 6\%$ for $n_{e0} = 0.015n_c$. However, the SRBS can still grow well with $\delta n_{e0}/n_{e0} = 10\%$, as shown in Table I. Actually, SRBS is suppressed but not fully broken down by the density fluctuation because there are always plasma regions satisfying $\delta\omega < 2\gamma$ [26].

The optimal 2D simulation results of the self-compression regime are shown in Fig. 4. An initial SRBS amplitude of $b_n \sim 3 \times 10^{-5}$ is obtained by inverse fast Fourier transform of the wavelength from 1100 nm to 1200 nm. After $2000\,T$, the pump starts to be depleted as the nonlinear stage is achieved, as shown in Fig. 4(a). The plasma wave produces longitudinal electric field, so it can be described by E_z, which contains clear periodic structures at $t = 2000\,T$, as shown in Fig. 4(b). The plasma wave (E_z) has several spikes with decreasing peak intensity from the main spike, indicating the typical feature of the π pulse in the nonlinear stage [2]. The peak SRBS amplitude grows from near 0 to 0.066 after 4-mm amplification, as shown in Fig. 4(c). The amplified SRBS beam slightly diverges from 10 μm to 20 μm, showing a much smaller diverge angle than the pump focus. The total transfer efficiency is about 18%. After considering the extra interaction length L of ~0.85 mm according to Eqs. (4) and (5) for the PIC simulation, it is reduced to about 16%. This efficiency may not satisfy the demand of pettwatt laser facilities [27]. It can be enhanced by using a longer pump duration because the nonlinear stage has been reached. Moreover, the transfer

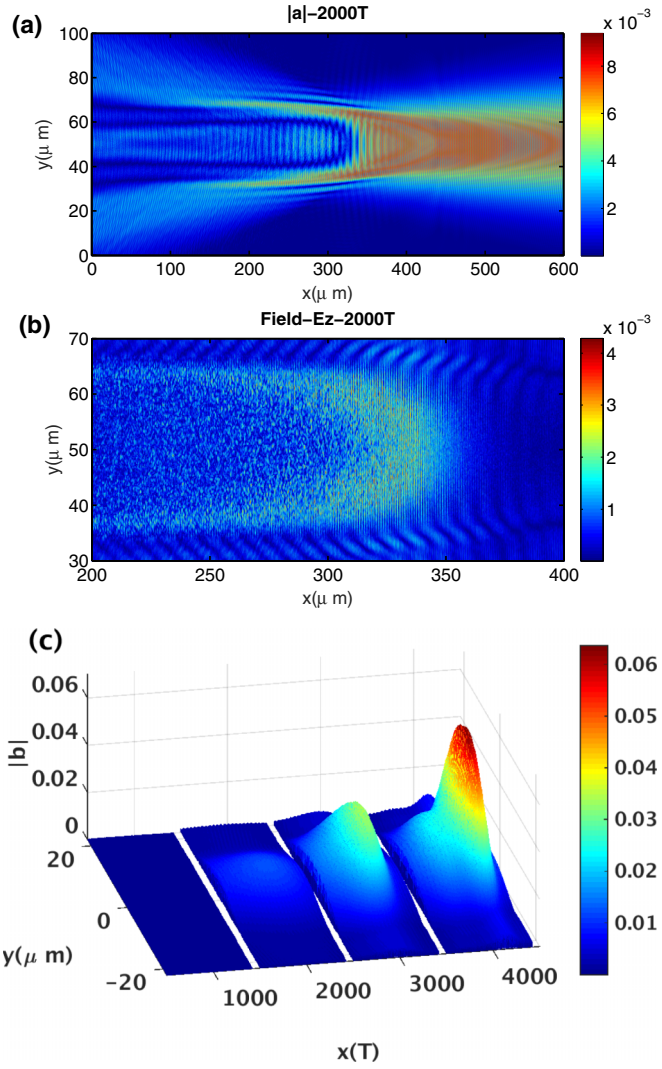

FIG. 4. The optimal 2D simulation results of the seedless BRA with flying focus, for $n_{e0} = 0.015n_c$. (a) Profile of the normalized pump amplitude at $t = 2000\,T$. (b) Structure of plasma wave (E_z) at $t = 2000\,T$. (c) Profiles of the SRBS amplitude ($|b|$) at different interaction time.

efficiency can be higher by replacing the Gaussian focal spot with a super-Gaussian one because the beam edge in the simulation only has ~1/10 of the transfer efficiency as the beam center. In addition, as plasma noise can almost perfectly match the resonant frequency and spatiotemporal synchronization with the pump pulse, probably the noisy seed can lead to an even higher transfer efficiency than a prepared short seed. For instance, the highest efficiency reported by plasma-based Raman amplifiers so far is from the experimental result of plasma noise [28].

The simulation results with a well-synchronized short seed and a long-duration seed are displayed in Fig. 5. Both the long and short seeds have a central wavelength 1140 nm, a peak amplitude of 0.001, and a beam waist of 100 μm (for a Rayleigh length more than 4 mm). The long seed with a full width at half maximum (FWHM) duration of 2 ps fully covers the moving window while the short seed with a FWHM duration of 200 fs locates at 400 μm of the moving window.

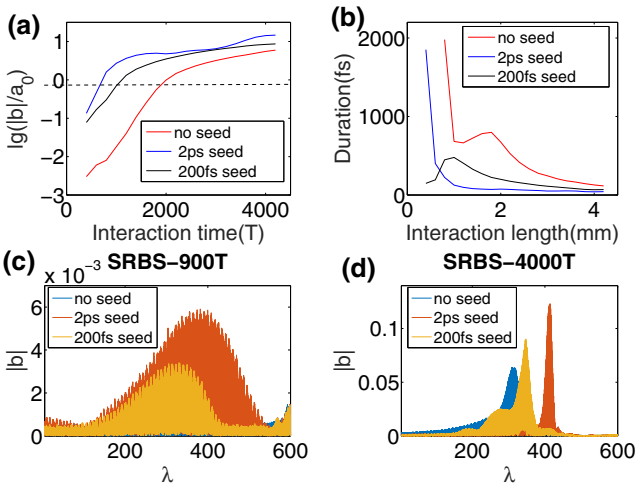

FIG. 5. Simulation results of (a) peak intensity and (b) FWHM duration with a 2-ps seed, a 200-fs seed, and plasma noise. (c) On-axial pulse shapes of SRBS at $t = 900\,T$. (d) On-axial pulse shapes of SRBS at $t = 4000\,T$.

As shown in Fig. 5(a), although the initial amplitude of the plasma noise is $1/30$ of the seeds, their amplitudes are comparable after the 4-mm amplification. This is mainly due to the growth rate γ degrading from exponentially to near linearly after the pump is depleted. Despite a strong seed leads to an earlier nonlinear stage, the growth rate would then drop and thereby the amplified intensity is approached by the noisy seed. The evolution of pulse duration is displayed in Fig. 5(b): Both the noise and 2-ps seed can be directly compressed in the linear stage, implying they are effective as the 200-fs short seed. In the nonlinear stage, all pulses are further compressed to 116 fs, 65 fs, and 40 fs by the plasma noise, the 200-fs seed, and the 2-ps seed, respectively.

IV. DISCUSSION

The best result is obtained by the long-duration seed, with an output peak amplitude and a transfer efficiency of 0.12 and 28.3%, respectively, which are higher than 0.09 and 24.4% obtained by the case of short seed. This is mainly due to a better envelope match of the SRBS maximum with gain maximum. The concept of envelope match has been proposed in the seed-ionizing BRA [19]. Here a similar regime is shown by using a long-duration seed and a flying focus. In the linear stage, the SRBS maximum has a subluminal speed [2], a long-duration seed can accelerate the maximum moving by providing a plasma wave to the following interaction region from the pulse front. Therefore, the linear amplified seed peak is nearer to the pump focus (400λ) than that of the short seed, as shown in Fig. 5(c). Conversely, in the nonlinear stage when the SRBS peak has a superluminal velocity [2], the acceleration of the SRBS maximum moving becomes a negative factor. However, this issue can be overcome here because the SRBS cannot be faster than the flying focus. As shown in Fig. 5(d), the amplified peak of the 2-ps seed still locates at 400λ. Therefore, different from the previous conclusion that a short seed with a sharp front is preferred for BRA, a long-duration seed here leads to an even better result.

Another issue of the flying focus is the limitation of interaction aperture. To mitigate precursors and plasma preheating, it requires producing an ionization wave a short distance in front of the SRBS [14]. Commonly, the Rayleigh length of the pump focus has to be short or the intensity would be sufficiently strong to generate plasma far ahead of the beam waist. For instance, a Gaussian beam would have $z_R = w_0^2/\lambda \approx 6.4$ mm for $w_0 = 100\,\mu$m, $\lambda = 1\,\mu$m, where w_0 is the beam waist, so the pump would produce plasma 6.4 mm ahead of the flying focus. As a result, both the precursors and plasma preheating cannot be mitigated. Also, it cannot be used for self-compression. To solve the problem, a random phase plate can be employed before the achromatic lens to magnify the beam waist without changing the Rayleigh length. In principle, the phase plate would only influence the wave front but not the achromatic aberration. Moreover, the amplified SRBS shows a much smaller diverge angle than the flying pump focus, as shown in the simulation result of Fig. 4(c) with only a $5\,\mu$m pump focal spot, implying the amplified SRBS has a different spatial model as the pump focus would not diffract out. The phase plate is widely used in large laser facilities for a beam waist more than 200 μm [29]. To further enlarge the beam focus to millimeter or centimeter, a microlens array can be used to merge a series of small focus into a large one.

V. CONCLUSION

In summary, we presented 2D PIC simulations about the self-compression regime of BRA with a flying focus. By employing the flying focus with velocity around $-c$ into the PIC code Opic2D, the simulation result displayed that the SRBS developing from plasma noise can far exceed that of the pump intensity, with a transfer efficiency around 16% after 5 mm interaction. Moreover, a long-duration seed leads to an even better result than a short seed by improving the envelope match of the SRBS maximum with gain maximum. As only one laser pulse is used in the simulation, the results provide a significant way for the simplification of plasma-based Raman amplifiers.

ACKNOWLEDGMENTS

This work was partly supported by National Key Program for S&T Research and Development (Grant No. 2018YFA0404804), the National Natural Science Foundation of China (Grant No. 11875240).

[1] D. Strickland and G. Mourou, Opt. Commun. **56**, 219 (1985).

[2] V. M. Malkin, G. Shvets, and N. J. Fisch, Phys. Rev. Lett. **82**, 4448 (1999).

[3] V. M. Malkin, G. Shvets, and N. J. Fisch, Phys. Rev. Lett. **84**, 1208 (2000).
[4] G. A. Mourou, N. J. Fisch, V. M. Malkin, Z. Toroker, E. A. Khazanov, A. M. Sergeev, T. Tajima, and B. L. Garrec, Opt. Commun. **285**, 720 (2012).
[5] Y. Ping, W. Cheng, S. Suckewer, D. S. Clark, and N. J. Fisch, Phys. Rev. Lett. **92**, 175007 (2004).
[6] W. Cheng, Y. Avitzour, Y. Ping, S. Suckewer, N. J. Fisch, M. S. Hur, and J. S. Wurtele, Phys. Rev. Lett. **94**, 045003 (2005).
[7] J. Ren, S. Li, A. Morozov, S. Suckewer, N. A. Yampolsky, V. M. Malkin, and N. J. Fisch, Phys. Plasmas **15**, 056702 (2008).
[8] A. A. Andreev, C. Riconda, V. T. Tikhonchuk, and S. Weber, Phys. Plasmas **13**, 053110 (2006).
[9] L. Lancia, J. R. Marquès, M. Nakatsutsumi, C. Riconda, S. Weber, S. Hüller, A. Mančić, P. Antici, V. T. Tikhonchuk, A. Héron, P. Audebert, and J. Fuchs, Phys. Rev. Lett. **104**, 025001 (2010).
[10] L. Lancia, A. Giribono, L. Vassura, M. Chiaramello, C. Riconda, S. Weber, A. Castan, A. Chatelain, A. Frank, T. Gangolf, M. N. Quinn, J. Fuchs, and J.-R. Marquès, Phys. Rev. Lett. **116**, 075001 (2016).
[11] J.-R. Marqués, L. Lancia, T. Gangolf, M. Blecher, S. Bolanos, J. Fuchs, O. Willi, F. Amiranoff, R. L. Berger, M. Chiaramello, S. Weber, and C. Riconda, Phys. Rev. X **9**, 021008 (2019).
[12] D. Turnbull, S. Li, A. Morozov, and S. Suckewer, Phys. Plasmas **19**, 073103 (2012).
[13] D. Turnbull, S. Li, A. Morozov, and S. Suckewer, Phys. Plasmas **19**, 083109 (2012).
[14] D. Turnbull, S. Bucht, A. Davies, D. Haberberger, T. Kessler, J. L. Shaw, and D. H. Froula, Phys. Rev. Lett. **120**, 024801 (2018).
[15] D. H. Froula, D. Turnbull, A. S. Davies, T. J. Kessler, D. Haberberger, J. P. Palastro, S.-W. Bahk, I. A. Begishev, R. Boni, S. Bucht, J. Katz1, and J. L. Shaw, Nat. Photonics **12**, 262 (2018).
[16] D. Turnbull, P. Franke, J. Katz, J. P. Palastro, I. A. Begishev, R. Boni, J. Bromage, A. L. Milder, J. L. Shaw, and D. H. Froula, Phys. Rev. Lett. **120**, 225001 (2018).
[17] D. Turnbull, S.-W. Bahk, I. A. Begishev, R. Boni, J. Bromage, S. Bucht, A. Davies, P. Franke, D. Haberberger, J. Katz, T. J. Kessler, A. L. Milder, J. P. Palastro, J. L. Shaw, and D. H. Froula, Plasma Phys. Control. Fusion **61**, 014022 (2019).
[18] Z. M. Zhang, X. T. He, Z. M. Sheng, and M. Y. Yu, Appl. Phys. Lett. **100**, 134103 (2012).
[19] Z. M. Zhang, B. Zhang, W. Hong, M. Y. Yu, J. Teng, S. K. He, and a. Y. Q. Gu1, Phys. Plasmas **21**, 123109 (2014).
[20] Z. M. Zhang, B. Zhang, W. Hong, Z. G. Deng, J. Teng, S. K. He, W. M. Zhou, and Y. Q. Gu, Phys. Plasmas **24**, 113104 (2017).
[21] A. Sainte-Marie, O. Gobert, and F. Quéré, Optica **4**, 1298 (2017).
[22] P. Franke, D. Ramsey, T. T. Simpson, D. Turnbull, D. H. Froula, and J. P. Palastro, Phys. Rev. A **104**, 043520 (2021).
[23] D. H. Froula, J. P. Palastro, D. Turnbull, A. Davies, L. Nguyen, A. Howard, D. Ramsey, P. Franke, S.-W. Bahk, I. A. Begishev, R. Boni, J. Bromage, S. Bucht, R. K. Follett, D. Haberberger, G. W. Jenkins, J. Katz, T. J. Kessler, J. L. Shaw, and J. Vieira, Phys. Plasmas **26**, 032109 (2019).
[24] V. M. Malkin, Z. Toroker, and N. J. Fisch, Phys. Plasmas **21**, 093112 (2014).
[25] M. Chiaramello, C. Riconda, F. Amiranoff, J. Fuchs, M. Grech, L. Lancia, J.-R. Marquès, T. Vinci, and S. Weber, Phys. Plasmas **23**, 072103 (2016).
[26] A. A. Balakin, D. S. Levin, and S. A. Skobelev, Phys. Rev. A **102**, 013516 (2020).
[27] D. Haberberger, A. Davies, J. L. Shaw, R. K. Follett, J. P. Palastro, and D. H. Froula, Phys. Plasmas **28**, 062311 (2021).
[28] G. Vieux, S. Cipiccia, D. W. Grant, N. Lemos, P. Grant, C. Ciocarlan, B. Ersfeld1, M. S. Hur, P. Lepipas, G. G. Manahan, G. Raj, D. R. Gil, A. Subiel, G. H. Welsh, S. M. Wiggins, S. R. Yoffe, J. P. Farmer, C. Aniculaesei, E. Brunetti1, and X. Yang, Sci. Rep. **7**, 2399 (2017).
[29] Y. Ping, R. K. Kirkwood, T.-L. Wang, D. S. Clark, S. C. Wilks, S. C. Wilks, N. Meezan, R. L. Berger, J. Wurtele, N. J. Fisch, V. M. Malkin, E. J. Valeo, S. F. Martins, and C. Joshi, Phys. Plasmas **16**, 123113 (2009).